Symplectic scheme and the Poynting vector in the reverse time migration

Edvaldo S. Araujo*, CPGG/UFBA, Reynam C. Pestana and Adriano W. G. dos Santos, CPGG/UFBA and INCT-GP/CNPQ

Abstract

In this work a new numerical solution for the wave equation based on the combination of the symplectic integrators and the expansion of the cosine function in a series of Chebyshev polynomials is presented. The method proposed here can march the wavefield in time, generating stable propagation of seismic waves free of numerical dispersion. Furthermore, the new numerical scheme provides the solution of the wave equation and its first time derivative without any increase in computational cost. Thus, the Poynting vector can also be calculated using this method in a more accurate procedure. Based on the Poynting vector information a new methodology is also proposed to separate the wavefields in its upgoing and downgoing components.

Through numerical examples, this work shows the applicability of the new method to extrapolate a wavefield with time steps larger than the ones commonly used by pseudo-spectral methods, as well as the ability of this symplectic method to successfully handle Poynting vector calculations.

Introduction

In the literature, the reverse time migration (RTM) has been implemented by solving the wave equation through various mathematical methods. Among the explicit methods, we have: finite differences (FD), which makes use of the Taylor expansion (Etgen, 1986); the rapid expansion method (REM), which makes use of the Chebyshev expansion (Kosloff et al., 1989; Pestana and Stoffa, 2010) and the two-step explicit marching method, which makes use of a polynomial expansion (Soubaras and Zhang, 2008). Symplectic integrators are another class of methods that can also be used in RTM.

In mathematics, a symplectic integrator is a numerical integration scheme for a specific group of differential equations related to classical mechanics and symplectic geometry (Yoshida, 1990). Symplectic integrators form a subclass of geometric integrators which, by definition, are canonical transformations. These schemes are widely used in molecular dynamics, celestial mechanics and other areas of physics. In the RTM, symplectic schemes can also be used to calculate the analytical solution of the wave equation and its first time derivative. One aspect of symplectic schemes is that the calculated wavefield is used to compute the time derivative of the wavefield at the same time step. The use of both wavefileds is useful for absorbing boundary conditions as mentioned by Bonomi et al. (1998). The symplectic schemes are also an interesting option for calculating the Poynting vector, since these numerical methods already provide the time derivative of the wavefield without any increase in computational cost.

In this paper, we present a new numerical method to extrapolate the wavefield in the RTM. The proposed method is symplectic and utilizes the rapid expansion method. It also shows a new procedure using the Poynting vector to separate the wavefield of common shot gathers, before carrying out the imaging condition in reverse time migration. Furthermore, it presents the results of using RTM symplectic integrator combined with REM.

Symplectic schemes for the acoustic wave equation

A Hamiltonian system is a system of equations in the following form (Chen, 2009):

$$\begin{aligned} \frac{d\vec{x}}{dt} &= \frac{\partial H}{\partial \vec{p}}\,, \\ \frac{d\vec{p}}{dt} &= -\frac{\partial H}{\partial \vec{x}}\,, \end{aligned} \tag{1}$$

where $\vec{x}$ and $\vec{p}$ are n-dimensional vectors of generalized coordinates and moments, respectively, t is the independent time variable and $H = H(\vec{x},\vec{p})$ is the Hamiltonian function. The set of coordinates of the position and momentum $(\vec{x},\vec{p})$ are called canonical coordinates.

Considering a system of differential equations governed by the Hamiltonian

$$H(\vec{x},\vec{p}) = T(\vec{p}) + V(\vec{x})\,, \tag{2}$$

where $T(\vec{p})$ is the kinetic energy and $V(\vec{x})$ is the potential, the equations of motion for a unit mass particle is given by:

$$\begin{aligned} \frac{d\vec{x}}{dt} &= \frac{\partial H}{\partial \vec{p}} = \vec{p}\,, \\ \frac{d\vec{p}}{dt} &= -\frac{\partial H}{\partial \vec{x}} = \vec{f}\,, \end{aligned} \tag{3}$$

where $\vec{f}$ is the force vector and $\vec{p}$ is the moment vector.

The constant density acoustic wave equation

$$\frac{\partial^2 P}{\partial t^2} = c^2 \nabla^2 P\,, \tag{4}$$

where $p = P(x,y,z,t)$ is the pressure wavefield and $c = c(x,y,z)$ is the wave propagation velocity in the medium, can also be rewritten using the Hamiltonian formulation (Bonomi et al., 1998) as:

$$\begin{aligned} \frac{\partial P}{\partial t} &= Q\,, \\ \frac{\partial Q}{\partial t} &= c^2\nabla^2 P\,. \end{aligned} \tag{5}$$

The wave equation (5) allows the use of a family of symplectic methods for the integration in time. According to Skell et al. (1997), symplectic methods preserve certain invariant of the Hamiltonian system, work with remarkable precision for long integration intervals and are stable for systems where linear extrapolation step size is sufficiently small.

Yoshida (1990) presented solutions (symplectic integrators) for equation (1) which can be also used for equation (5). One of these solutions is the Stomer-Verlet method:

$$\begin{aligned} Q^{(n+\frac{1}{2})} &= Q^{(n)} + \frac{1}{2}\Delta t c^2\nabla^2 P^{(n)}\,, \\ P^{(n+1)} &= P^{(n)} + \Delta t Q^{(n+\frac{1}{2})}\,, \\ Q^{(n+1)} &= Q^{(n+\frac{1}{2})} + \frac{1}{2}\Delta t c^2\nabla^2 P^{(n+1)}\,. \end{aligned} \tag{6}$$

However, the time interval Δt used in the discretized equations (5) should be small enough to achieve stability and avoid numerical dispersion. To overcome this issue, we present a new numerical method that originates from the analytical solution of equation (4) (Araujo and Pestana, 2010; Pestana and Stoffa, 2010) that is given by:

$$P(t+\Delta t) + P(t-\Delta t) = 2\cos(L\Delta t)P(t)\,, \tag{7}$$

with $L^2 = -c^2\nabla^2$.

Using the REM (Kosloff et al., 1989) in (7), results to:

$$\begin{aligned} &P(t+\Delta t) + P(t-\Delta t) \\ &= 2\sum_{(k=0)}^{M} C_{2k} J_{2k}(\Delta t R)\, Q_{2k}\left(\frac{iL}{R}\right) P(t)\,, \end{aligned} \tag{8}$$

being $C_0 = 1$ and $C_k = 2$ for $k \neq 1$. J_k is the Bessel function of order k, Q_k are the modified Chebyshev polynomials and for $2D$ wave propagation, the value of R is given approximately by: $R = \pi c_{max}\sqrt{\left(\frac{1}{\Delta x}\right)^2 + \left(\frac{1}{\Delta z}\right)^2}$, where c_{max} is the maximum velocity in the mesh and Δx and Δz are the grid spacings (Tal-Ezer, 1986).

Equation (7) can now be rewritten as

$$\frac{\partial P}{\partial t} = Q\,, \qquad \text{and} \qquad \frac{\partial Q}{\partial t} = H(P)\,, \tag{9}$$

with

$$H(P) = \frac{2}{(\Delta t)^2}[\cos(L\Delta t) - 1]\,P\,. \tag{10}$$

Using the REM and the Stomer-Verlet method in equation (9) a new numerical method called Stomer-Verlet-REM is formulated i.e.:

$$\begin{aligned} P^{(n+1)} &= P^{(n)} + \Delta t Q^{(n)} + \frac{\Delta t^2}{2} G(P^{(n)})\,, \\ Q^{(n+1)} &= Q^{(n)} + \frac{\Delta t}{2}[G(P^n) + G(P^{(n+1)})]\,, \end{aligned} \tag{11}$$

where

$$G(P^{(n)}) = \frac{2}{(\Delta t)^2}\left[\sum_{(k=0)}^{M} C_{2k} J_{2k}\, Q_{2k} - 1\right] P^{(n)}\,. \tag{12}$$

The numerical scheme (11) behaves similarly to the scheme (8) with respect to the use of Chebyshev expansion. It is only necessary to calculate the expansion twice for the first time step. The method provides both the wavefield $P^{(n+1)}$ and the derivative of the wavefield with respect to time, which is $Q^{(n+1)}$. Furthermore, it is interesting that the calculated wavefield $P^{(n+1)}$ is used in the same time step to calculate $Q^{(n+1)}$. This characteristic allows a mechanism to reverse the direction of propagation of the wavefield and it can be useful for absorbing boundary conditions (Bonomi et al., 1998).

In expression (12) one must ensure that the number of terms used by the Chebyshev expansion provides a good approximation of the cosine function such that the wavefield extrapolation can occur in a stable form. Tal-Ezer (1986) mentions that the Chebyshev expansion converges for $M \geq R\Delta t$.

Other families of symplectic integrators with different integration orders can be used in the equation (9). The higher the order, the more accurate is the result, i.e., the numerical solution is closer to the exact solution.

To demonstrate the applicability and efficiency of the proposed symplectic method, we implemented equations (11) and (12) and we migrated the Marmousi synthetic dataset. The velocity field mesh has 369 points in the horizontal direction (x) and 375 in the vertical direction (z) and the spacings are $\Delta x = 25$ m and $\Delta z = 8m$. Figure 1 shows the result of pre-stack RTM for the Marmousi model. The result of the RTM using the 240 shot gathers shows that the numerical algorithm performed well and produced a successful result for the Marmousi model. Furthermore, the symplectic scheme used a time sampling interval of $4ms$, which is the original time interval of this seismic dataset, and it did not present any stability issues neither numerical dispersion, once it uses REM for approximating the $cos(L\Delta t)$ function.

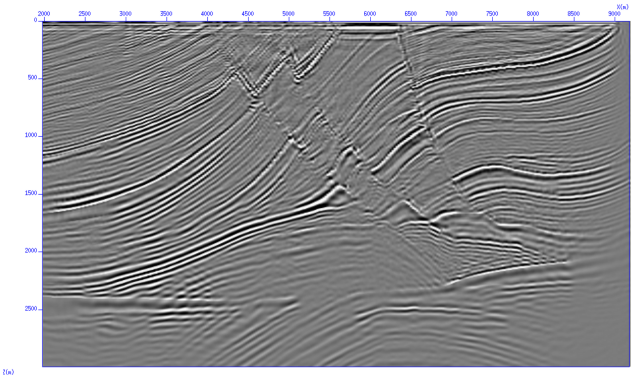

Figure 1: Migration result of the Marmousi model using the proposed symplectic method based on the solution of equations (11) and (12).

Poynting vector applications

The symplectic schemes are of great interest for pres-stack RTM. Normally, in this type of migration, the imaging condition used is the zero-lag cross-correlation between the extrapolated source wavefield and backward propagated receiver wavefield. This type of imaging condition correlates all kinds of wave, including head

waves and turning waves which are neither derived from reflections nor from backscattering waves. The correlation of these waves generates artifacts in the migrated image (Yoon and Marfurt, 2006). In order to eliminate these artifacts, several strategies have been presented in the literature. Yoon and Marfurt (2006) developed a filter based on the Poynting vector and Bulcão (2004) presented the idea of using the Poynting vector to separate the wavefield in its ascending and descending components and use only the descending part in the imaging condition.

In order to calculate the Poynting vector $\vec{S}$, the time derivative of the wavefield and its gradient need to be computed and it is given by (Bonomi et al., 1998):

$$\vec{S} = -Q\nabla P\,. \tag{13}$$

The symplectic schemes have naturally provided the time derivative of the wavefield with good accuracy. So, it is only necessary to calculate the gradient field to obtain the Poynting vector accurately.

Figure 2(a) shows a small part of the BP model, which is a structurally complex model containing a salt body in the middle of the model. Figure 2(b) presents a snapshot of the source wavefield computed using the BP model. Figures 3(a) and 3(b) show the snapshots of the components of Poynting vector $\vec{S}$ at the same instant for the snapshot shown in Figure 2(b).

In the work presented by Bulcão (2004), one uses the Poynting vector and the normalized derivative of the energy to make the separation of the wavefield. In this paper, we present a new form of separating the wavefield. For this, we calculate the angle of the direction of propagation of the wavefield, through the Poynting vector, i.e.:

$$\theta = \arctan\left(\frac{S_z}{S_x}\right)\,. \tag{14}$$

The ascending part of the wave field is considered where $\theta \in [0;\pi]$ and the descending wave for $\theta \in [0;-\pi]$. With these definitions, one can select the part of the wavefield of interest. The great advantage of this procedure is that it does not alter the amplitudes of the wavefield. Figures 4(a) and 4(b) show the results of the application of this methodology in the wavefield at a given instant of time and show the result of applying this technique for the snapshot of Figure 2(b).

The Poynting vector can also be used to generate common image gathers (CIGs) in the reflection angle domain. Figure 5 shows some CIGs in the angle domain for a small part of the 2004 BP 2D dataset. As the correct velocity model was used to migrate this dataset, a good continuity of events can be observed in the horizontal direction.

Numerical results

A very common procedure to remove the low frequency noise present in the RTM images is to generate CIGs in the reflection angle domain and stack only the angles that are not contaminated by the low frequency noise, which are produced by the cross-correlation imaging condition. Using the symplectic scheme combined with the REM we can obtain source and receiver extrapolated wavefileds and generate the CIGs through the application of the Poynting vector. To test and validate the method proposed here,

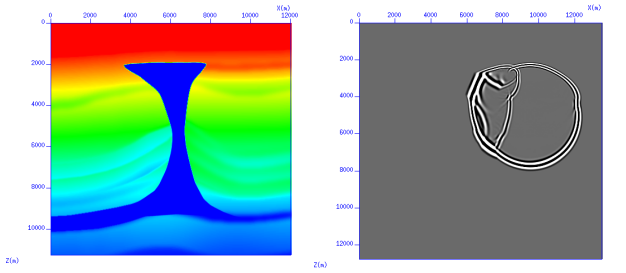

(a) (b)

Figure 2: (a) Salt dome part of the BP model and (b) a source wavefield snapshot.

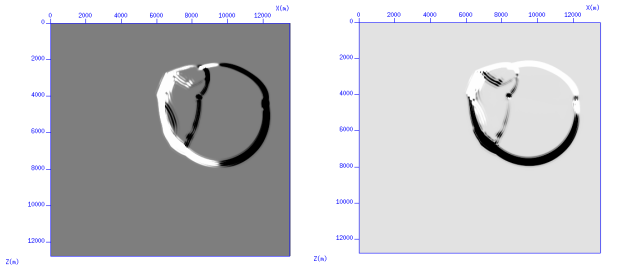

(a) (b)

Figure 3: Poynting vector components computed using the BP Model: (a) S_x and (b) S_z.

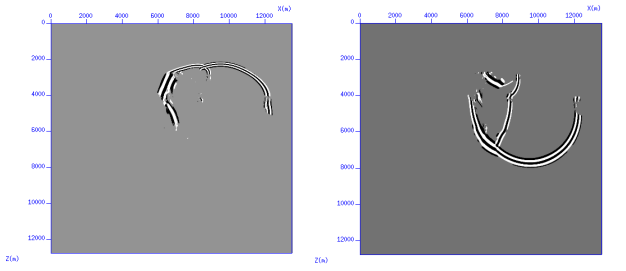

(a) (b)

Figure 4: Separated wavefieds: (a) upgoing and (b) downgoing wavefields

we use the BP 2D model 2004. Figure 6 shows the migration result of the 2004 BP 2D dataset using the CIGs reflection angles from 0° to 60°. Figure 7 shows the image using the reflection angles in the range between 61° and 90°. As we can see most of the low frequency noise is concentrated in the higher reflection angles. However, the image obtained by stacking all CIGs in the range from 0° to 60° attenuated some reflections above the salt. To recover these reflections, a high pass filter was applied to the CIGs in the range from 61° to 90° and stacking these CIGs we obtained the result shown in the Figure 8. Thus, combining the results shown in Figures 6 and 8, we obtain the final migrated image (Figure 9) that shows a clearer image free of low frequency noise. This procedure takes advantage of information that are usually discarded to attenuate low-frequency artifacts in the image migrated from RTM.

Conclusions

The new symplectic numerical scheme presented in this work proved to be a good alternative to RTM. The method is not limited to a certain range of temporal sampling and has no problem with numerical dispersion and stability.

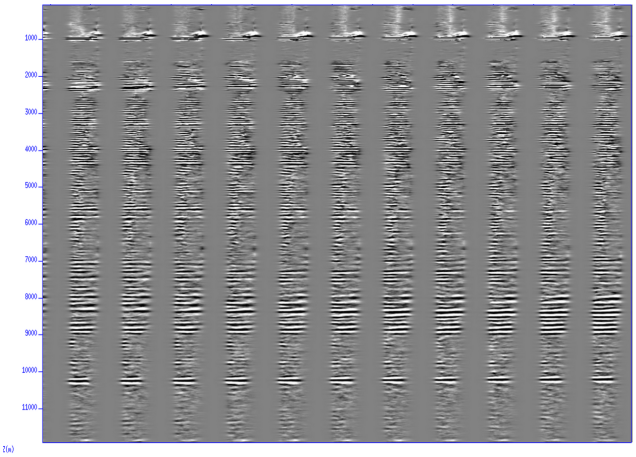

Figure 5: Some common image gathers in the reflection angle domain from the 2004 BP dataset (reflection angles 0° to 60°).

Furthermore, it allows a more accurate calculation of the Poynting vector, since this scheme has naturally provided the time derivative of the wavefield.

This work also presented a new methodology for separation of the wavefield in any direction using the desired angular aperture obtained from the computation of the angle of propagation of the wavefield through the Poynting vector. One advantage of this technique is that the amplitude of the wave field is not changed during the separation process. Thus, the descendents wavefieds of the source and receivers can be used in the imaging condition in order to improve the quality of the migrated image section.

The strategy of using the reflection angles between 61° and 90°, which is usually discarded, is important to image structures which are masked by noise, especially in shallow regions of complex geological models.

Acknowledgements

The authors thank CPGG/UFBA, CNPq and INCT-GP/CNPq for supporting the development of this work. Also CAPES for its support through a doctorate grant.

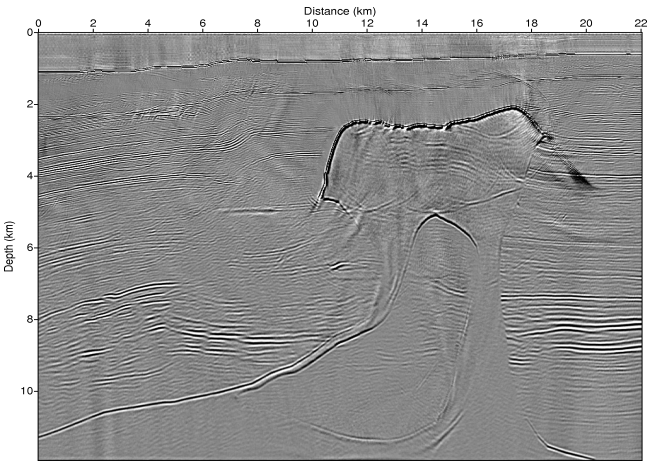

Figure 6: Migration result of the 2004 BP 2D dataset using the CIGs reflection angles from 0° to 60°.

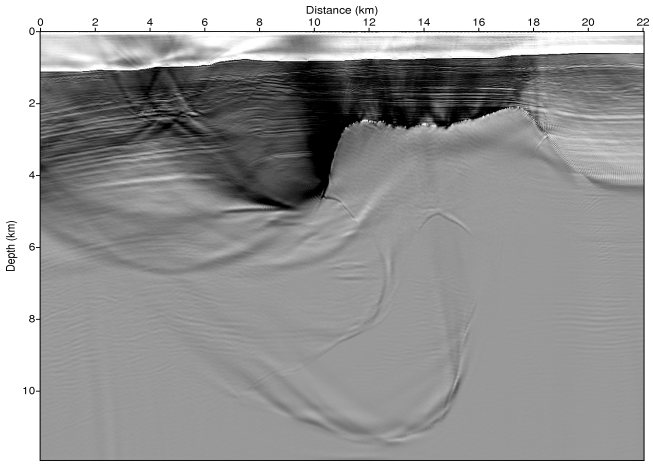

Figure 7: Migration result of the 2004 BP 2D dataset using the CIGs reflection angles from 61° to 90°.

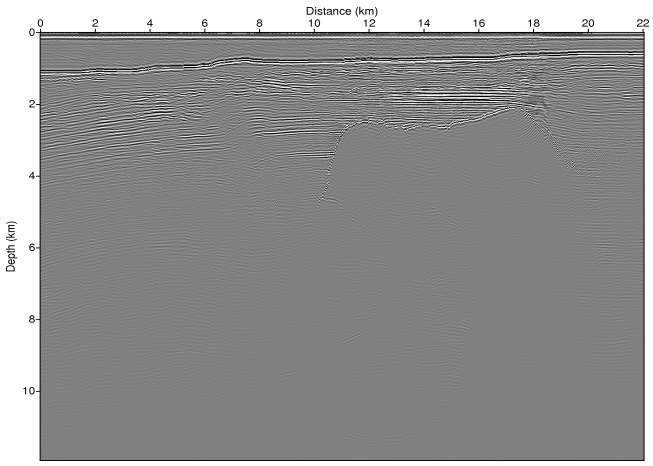

Figure 8: Migration image of the 2004 BP 2D dataset using the CIGs reflection angles from 61° to 90° after high pass filtering.

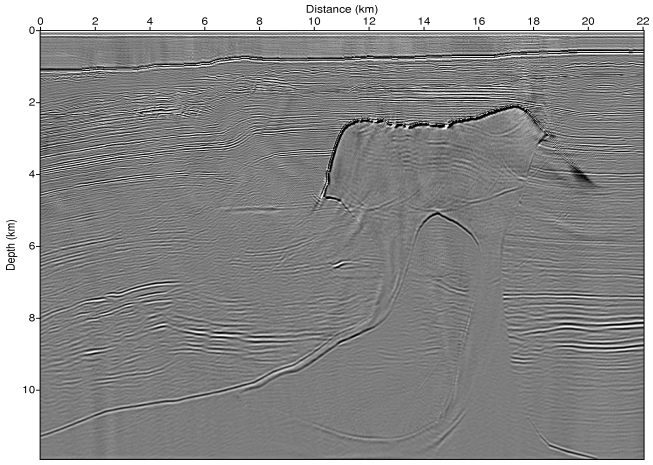

Figure 9: Final migration result obtained by summing the CIGs reflection angles shown in Figure 6 and Figure 8.

References

Araujo, E. S. and R. C. Pestana, 2010, Análise dos métodos de diferenças finitas e expansão rápida na migração reversa no tempo: RBGf, **28(4)**, 723–739.

Bonomi, E., L. Brieger, C. Nardone, and E. Pieroni, 1998, 3d spectral reverse time migration with no-wraparound absorbing conditions: Geophysics Area CRS4.

Bulcão, A., 2004, Modelagem e migração reversa no tempo empregando operadores elásticos e acústicos: Tese de Doutorado-UFRJ:PEC/COPE.

Chen, J., 2009, Lax-wendroff and nystrom methods for seismic modeling: Geoph. Prosp., **57**, 931–941.

Etgen, J., 1986, High-order finite-difference reverse time migration with the 2-way non-reflecting: SEP48:, 133–146.

Kosloff, D., A. Filho, E. Tessmer, and A. Behle, 1989, Numerical solution of the acoustic and elastic wave equation by new rapid expansion method: Geoph. Prosp., **37**, 383–394.

Pestana, R. C. and P. L. Stoffa, 2010, Time evolution of the wave equation using rapid expansion method: Geophysics, **75**, 121–131.

Skell, R. H., G. Zhang, and T. Schlick, 1997, A family of symplectic integrators: stability, accuracy, and molecular dynamics applications, society of industrial and applied mathematics: J. on Numerical Analysis, **18**, 203–222.

Soubaras, R. and Y. Zhang, 2008, 2008: In: 70th EAGE Conference and Exhibition,Rome/Italy, EAGE.

Tal-Ezer, H., 1986, Spectral methods in time for hyperbolic problems. society of industrial and applied mathematics.: J. on Numerical Analysis, **23**, 11–20.

Yoon, K. and K. J. Marfurt, 2006, Reverse-time migration using the poynting vector: Explo. Geoph., **37**, 102–107.

Yoshida, H., 1990, Construction of higher order symplectic integrators: Physics Letters A, **150**, 262–268.